Electronic structure and magnetic properties of RMnX ($R =$ Mg, Ca, Sr, Ba, Y; $X =$ Si, Ge) studied by KKR method

V. Klosek[1], J. Toboła[1,2], A. Vernière[1], S. Kaprzyk[2], and B. Malaman[1] [a]

[1] Laboratoire de Chimie du Solide Minéral, Université Henri Poincaré - Nancy I, Associé au CNRS (UMR 7555), BP 239, F-54506 Vandoeuvre-lès-Nancy Cedex, France

[2] Faculty of Physics and Nuclear Techniques, AGH University of Science and Technology, Al. Mickiewicza 30, 30-059 Kraków, Poland

Abstract. Electronic structure calculations, using the charge and spin self-consistent Korringa- Kohn-Rostoker (KKR) method, have been performed for several RMnX compounds (R = Mg, Ca, Sr, Ba, Y; X = Si, Ge) of the CeFeSi-type structure. The origin of their magnetic properties has been investigated emphasizing the role of the Mn sublattice. The significant influence of the Mn-Mn and Mn-X interatomic distances on the Mn magnetic moment value is delineated from our computations, supporting many neutron diffraction data. We show that the marked change of μ_{Mn} with the Mn-Mn and Mn-X distances resulted from a redistribution between spin-up and spin-down d-Mn DOS rather than from different fillings of the Mn 3d-shell. The obtained KKR results are discussed considering the Stoner-like and covalent magnetism effects. From comparison of electronic structure of RMnX in different magnetic states we conclude that the antiferromagnetic coupling in the Mn (001) plane considerably increases the Mn magnetic moment with respect to the ferromagnetic arrangement. Bearing in mind that the neutron diffraction data reported for the RMnX compounds are rather scattered, the KKR computations of μ_{Mn} are in fair agreement with the experimental values. Comparing density of states near E_F obtained in different magnetic orderings, one can notice that the entitled RMnX systems seem to 'adapt' their magnetic structures to minimize the DOS in the vicinity of the Fermi level. Noteworthy, the SrMnGe antiferromagnet exhibits a pseudo-gap behaviour at E_F, suggesting anomalous electron transport properties. In addition, the F-AF transition occurring in the disordered La$_{1-x}$Y$_x$MnSi alloy for the $0.8 < x < 1$ range is well supported by the DOS features of La$_{0.2}$Y$_{0.8}$MnSi. This latter result sheds light on the magnetic structure of the YMnSi compound. In contrast to the investigated RMnX compounds, YFeSi was found to be non-magnetic, which is in excellent

1 Introduction

Among the equiatomic RTX compounds (R = rare or alkaline earth; T = transition element; X = metalloid), manganese is the only d element that exhibits a magnetic moment [1,2]. Thus $RMnX$ representatives allow for investigations of $3d$ itinerant magnetism in the RTX phases.

The structural and magnetic properties of the CeFeSi-type $RMnX$ (R = La - Tb (or Sm), Y, Mg - Ba) silicides and germanides have been extensively studied during the last decade, especially by means of X-ray diffraction, magnetic measurements, and neutron powder diffraction [1,2,3,4,5,6,7,8,9,10]. The CeFeSi-type structure (Table 1, Fig. 1) is closely related to the well-known $ThCr_2Si_2$-type structure. Both CeFeSi- (P4/nmm) and $ThCr_2Si_2$-(I4/mmm) types are characterised by the occurrence of 'BaAl4' slabs which consist in a stacking along the c axis of R, X, and T_2 (001) square planes with the sequence $R - X - T_2 - X - R$ (Fig. 1). In the CeFeSi structure, the 'BaAl$_4$' slabs are connected via $R - R$ contacts constituting a 'W' slab. The T atom ($CN12$) has a close coordination of four X atoms building a tetrahedron, and a second coordination shell constituted of four R atoms building a second tetrahedron. Four T atoms, building a square plane, complete the neighbourhood of T.

Neutron diffraction studies have shown that, in both CeFeSi-type $RMnX$ and $ThCr_2Si_2$-type RMn_2X_2 compounds, the magnetic behaviour of the Mn sublattice strongly depends on the Mn-Mn (d_{Mn-Mn}) and Mn-X (d_{Mn-X})

^{a} *Corresponding author:* Bernard.Malaman@lcsm.uhp-nancy.fr

interatomic distances. From many experimental studies one can notice that, within the (001) planes, the Mn-Mn coupling is ferromagnetic (F) for $d_{Mn-Mn} < 2.84$ Å and antiferromagnetic (AF) for $d_{Mn-Mn} > 2.89$ Å whereas complex magnetic arrangement (coexistence of F and AF components) occurs for intermediate distances. Nevertheless, the case of MgMnGe ($d_{Mn-Mn} = 2.79$ Å and AF Mn (001) planes) partly questions this metric criterion. On the other hand, the evolution of the μ_{Mn} moment in the $RMnX$ compounds is well interpreted when plotting μ_{Mn} versus the contraction rate (*with respect to the sum of the Mn and X ionic radii*) of d_{Mn-X} distance [see Fig. 6 of Ref. [5]]. The largest values of the Mn magnetic moment are observed in the compounds characterised by the largest Mn-X and Mn-Mn distances [4,6,7,8].

The aim of this paper is to investigate theoretically the magnetic properties of the Mn sublattice in the CeFeSi-type $RMnX$ silicides and germanides, from electronic structure calculations. We mainly focus on the dependency of the Mn magnetic moment value versus the Mn-Mn and Mn-X interatomic distances as well as on the relationships between the electronic states in the vicinity of the Fermi level (E_F) and the magnetic structure type.

Furthermore, the influence of the nature of the transition metal on magnetic properties onset has been analysed through electronic structure calculations of the YTSi (T= Cr, Mn, Fe) compounds.

2 Computational details

The electronic structure and ground state properties of the RMnX silicides and germanides have been calculated using the Korringa-Kohn-Rostoker (KKR) method [11,12,13]. Both core states and valence states are calculated self-consistently. The crystal potential of muffin-tin (MT) form is constructed within the local spin density approximation (LSDA) with the Barth-Hedin expression for the exchange-correlation potential [14]. The self-consistency cycles is repeated for each compound until the difference between the input and output crystal potentials is of about 1 mRy.

We have carried out the KKR calculations for the MgMnGe, CaMnGe, SrMnGe, BaMnGe, CaMnSi and YMnSi compounds in (i) ferromagnetic structure (F) (ii) three types of antiferromagnetic structures namely antiferromagnetic Mn (001) planes coupled either antiferromagnetically (AFI) or ferromagnetically (AFII) (see below), ferromagnetic Mn (001) planes coupled antiferromagnetically (AFIII). The non-spin polarised DOS have been also analysed to compare the Mn-DOS at E_F for the various Mn-Mn distances observed in the studied RMnX compounds. In the case of BaMnGe relativistic effects have been incorporated to compute core electronic states.

In the KKR calculations, the low temperature experimental values of the lattice parameters have been taken from the neutron diffraction data [4,5,8], whereas the atomic coordinates have been taken from the single crystal X-ray diffraction data [16] (Table 2). Noteworthy, for the YMnSi compound, the room temperature lattice parameters have been applied. Concerning the atomic coordinates, the values previously suggested for this compound (in fact those of the CeFeSi compound [15]) give a Mn-Si distance surprisingly short (2.35 Å) comparing to those observed for other RMnSi compounds [6]. So, in the following, we have used atomic positions extrapolated from Ref. [6], namely $z_Y = 0.67$ and $z_{Si} = 0.22$. In order to support this assumption, electronic structure of the La$_{0.2}$Y$_{0.8}$MnSi alloy ($\mathrm{d}_{Mn-Si} = 2.50$ Å) [7] was also studied by the KKR method incorporating the coherent potential approximation (CPA) to treat disorder.

The radii of the non-overlapping muffin-tin spheres have been chosen to obtain an optimal filling of the Wigner-Seitz cell (about 65-70%). One has to notice that moderate variations of the computational geometry did not affect our results. For the final crystal potentials, the total, site- and l-decomposed (with $l_{max} = 2$) densities of states (DOS) have been computed on a 601-energy-point mesh with a tetrahedral k-space integration technique using 375 small tetrahedra and 126 **k** points in the irreducible part of the Brillouin zone [17]. In the case of SrMnGe, electronic dispersion curves E(**k**) have been computed along high symmetry directions in the Brillouin zone.

The KKR-CPA cycles in La$_{0.2}$Y$_{0.8}$MnSi have been carried out in the complex energy plane using an elliptic contour and the Fermi level has been determined precisely via the generalized Lloyd formula [18].

In the presented figures the Fermi level (E_F) is taken as zero of the energy scale.

3 Results and discussion

3.1 Non spin-polarised DOS

The DOS curves of germanides and silicides obtained from non-spin-polarised calculations are displayed in Fig. 2. The lowest energy bands are mostly attributed to the metalloid s-states and are separated from the upper-lying states by a gap of about 0.2-0.3 Ry. These s-states are weakly hybridised with the other electronic states and all l-like DOS (seen on the R and Mn sites). They should be considered as the 'tails' of the X s-states and their role in bond formation can be neglected [19,20,21]. Moreover, we can note that the energy localization of the s-states increases when the size of the R element increases from Mg to Ba (Fig. 2). The expansion of the unit cell volume implies the increase of the $X - X$ interatomic distances and then the decrease of the overlaps of the X s-orbitals. Above the gap, the valence states are mostly of Mn $3d$ character. The Mn $3d$-states are strongly hybridised with the X p-states in the energy range of $-0.3 < E < -0.1$ Ry, yielding bonding states for Mn-X bonds. The corresponding antibonding states form a peak located c.a. 0.1 Ry above E$_F$. Note that the X p-orbitals contribute significantly to the bonding states while the antibonding states are essentially of Mn $3d$ character. This may originate from the energy barycentre of the X p-states lying lower than the one corresponding to the Mn $3d$ states. The electronic states occurring in the vicinity of E$_F$ mostly come from direct overlaps between the Mn $3d$ orbitals [20,21,22], corresponding to the (001) Mn planes (Fig. 1).

These states are located within a relatively narrow energy range, and there is no clear separation between bonding and antibonding states. The Mn-Mn bonds thus have a quite important metallic character and, anyway, they are less covalent than the Ti-Ti bonds calculated in the isotypic RTiX compounds (and even the Fe-Fe bonds, in the RFeSi compounds, see below) [22].

The electronic states projected on R sites give a little contribution to the density of states at the Fermi level. These states are dominated (except for MgMnGe) by d-states at higher energy range while there is a small admixture of s- and p-states at the lower energies. The hybridisation between the R s-, p- and d-states and the X p-states is rather important and there should be some bonding states for $R - X$ bonds. We can also note the hybridisation of R electronic states with the Mn $3d$ ones. This is particularly well seen in the case of the trivalent R element (YMnSi), where the shape of the $4d$ Y and $3d$ Mn DOS is quite similar in the energy range $-0.3 < E < +0.1$ Ry thus evidencing bonding states for Y-Mn bonds [23,24]. Conversely, the R-Mn bonds must be weaker in the RMnX compounds containing the divalent R elements, since the bonding states related to the R-Mn bonds are less filled.

In the case of YMnSi, the KKR results can be compared to the previous non-spin polarised LMTO calculations of Kulatov et al. [25] which are, to our knowledge, the only band theory results reported for the RMnX compounds. Despite of the overall agreement concerning the shape of non-polarised DOS, the present KKR calculations give a larger value of $n(E_F)$. However, we are not

aware of the crystallographic data used in the previous LMTO study.

Conclusively, the non-polarised KKR calculations of RMnX compounds show that the Fermi level is always located in the vicinity of large DOS peak originating essentially from $3d$-states on Mn. Moreover, the comparison of the computed DOS at E_F versus interatomic distances in RMnX compounds (Table 3) reveals that $n(E_F)$ increases regularly with increasing d_{Mn-Mn} (i.e. with the R size) but there is no apparent correlation between $n(E_F)$ and d_{Mn-X}. The electronic structure modifications with d_{Mn-Mn} can be roughly understood by smaller overlap of $3d$ orbitals, resulting in narrower bands and then enhanced density of states in the vicinity of the Fermi level.

In all investigated RMnX compounds, the computed $n(E_F)$ values for the Mn site are sufficiently large to satisfy the well-known Stoner limit $(In(E_F) > 1)$ for appearance of magnetism (Table 3). This may tentatively support the magnetic properties of the RMnX compounds (R= Y, Mg-Ba; X= Si, Ge) and led us to perform spin-polarised electronic structure calculations accounting for experimentally observed magnetic structures [3,4,5,8,10].

3.1.1 Non-magnetic properties of RFeSi

The origin of disappearance of magnetic properties in the RFeX compounds, unlike the aforementioned RMnX ones, can be tentatively illustrated when comparing e.g. the electronic structures of isotypic YFeSi, YMnSi and hypothetical YCrSi compounds (Fig. 3).

Using the lattice parameters of Ref. [16] ($a = 3.89$ Å, $c = 6.80$ Å) and the atomic positions extrapolated from Ref. [6] ($z_Y = 0.672$ and $z_{Si} = 0.185$), the KKR computations of YFeSi show that E_F is located on the strongly decreasing DOS. The obtained $n(E_F)$ value is as large as 80.8 states/Ry/f.u. (21.3 states/Ry for the Fe-site against 45.2 states/Ry for the Mn-site in YMnSi), which is below the Stoner limit (Table 3). Indeed, a highly accurate spin-polarised KKR computations also supported the non-magnetic ground state after a very slow convergence. This result is in very good accordance with the absence of magnetic moment on the iron site in all RFeSi series as deduced from ^{57}Fe Mössbauer studies [26].

Bearing that YFeSi is characterized by E_F located in the vicinity of large Fe d-DOS in mind, one suggests that this compound may be close to a magnetic instability. Thus, our theoretical results for YFeSi can not be immediately extrapolated to the other RFeX compounds and electronic structure of each RFeX compound has to be analysed individually. It is interesting to remind that non-magnetic properties of the structurally related ThCr$_2$Si$_2$-type LaFe$_2$Ge$_2$ compound have been previously supported by the LMTO calculations [27].

Similarly, high DOS at E_F has been computed in YCrSi (using extrapolated crystallographic parameters $a \approx 3.80$ Å, $c \approx 7.10$ Å, $z_Y \approx 0.65$, $z_{Si} \approx 0.24$), which also indicates that this compound is close to magnetic instability. Nevertheless, up to now, all attempts to stabilize RCrSi compounds have always failed.

Noteworthy, the $ThCr_2Si_2$-type YCr_2Si_2 compound was shown to exhibit a magnetic ordering from the neutron diffraction measurements [28].

4 Neutron diffraction results in R**Mn**X silicides and germanides (R = Mg-Ba)

The low temperature magnetic structures of the investigated RMnX compounds consist in antiferromagnetic (001) Mn planes coupled either ferromagnetically (MgMnGe, CaMnSi and CaMnGe [4,5,8], AFI structure) or antiferromagnetically (SrMnGe and BaMnGe [8], AFII structure) as shown in Fig. 4. We can notice that there exist some discrepancies between various experimental studies concerning both the reported magnetic structure and the refined value of Mn magnetic moment (Table 4).

Different orientations for the direction of the Mn magnetic moments have been reported for MgMnGe: either within the (001) plane [5] or along the c-axis [8]. The two magnetic models lead to different moment values at T= 2 K namely 3.3 μ_B and 2.9 μ_B, respectively. Similarly, in the case of CaMnGe the magnetic moments are along [001] according to [8] (μ_{Mn} = 3.80 μ_B), whereas they are tilted of about 34° from the c-axis according to [4] (μ_{Mn} = 3.34 μ_B). Some discrepancy also exists concerning the Mn magnetic moment value in CaMnSi. Although the Mn moments have been found to be aligned along the c-axis in both studies, their amplitudes are either 2.84 μ_B [8] or 3.27 μ_B [4].

The largest discrepancy between experimental works occurs in the case of BaMnGe. The Mn magnetic moment value has been refined to only 1.85 μ_B by Dascoulidou et al. [8] (a value strongly underestimated if comparing with other RMnX compounds) next corrected to 3.70 μ_B by Welter et al. in a further study [5]. According to these authors, the discrepancy simply results from an error in the normalization of the magnetic and nuclear intensities during the use of the Fullprof refinement software.

No neutron diffraction experiment has been carried out for the YMnSi compound. However, according to bulk magnetic measurements [3], a spontaneous magnetization is observed above 190 K ($M_s = 1.14\mu_B$) whereas an antiferromagnet is stabilized at 2 K. Later, a neutron study of the $La_{1-x}Y_x$MnSi solid solution [7] has concluded that a collinear ferromagnetic structure is likely for YMnSi above 200 K whereas antiferromagnetically coupled ferromagnetic (001) Mn planes characterize the 2K ordering. The $La_{0.2}Y_{0.8}$MnSi alloy was determined to be a pure ferromagnet with a Mn magnetic moment of 2.1(2) μ_B at 2K [7].

Remark : *It is worth noting that, in all neutron studies, the amplitude of the Mn moment are given with relatively large standard deviations (Table 4). As shown in the published neutron diffraction patterns and according to the magnetic structures [5,8], this is due to the lack of magnetic contributions which, furthermore, mostly occur under strong nuclear peaks.*

4.1 Spin-polarised DOS

4.1.1 RMnX (R=Mg-Ba)

Based on the aforementioned experimental results [4,5,7,8] the ground state electronic structure calculations were performed considering, first, a simple ferromagnetic state and next, accounting for the real magnetic ordering of Mn sublattices. We present DOS in ferromagnetic (Fig. 5) and antiferromagnetic states (Fig. 6), i.e. in the AFI structure for MgMnGe, CaMnGe, CaMnSi and in the AFII structure for SrMnGe and BaMnGe. Noteworthy, in the latter compounds the c lattice constant was doubled to allow for calculations of the AFII structure (Fig. 4).

First, let us compare KKR total energy computed in non-magnetic and different types of magnetic structure. We can roughly conclude (without presenting detailed analysis of all contributions to the total energy of the system) that our calculations always resulted in a preference of a magnetic state in all investigated RMnX compounds. Moreover, one observes much lower DOS at E_F in the AF state than in the F one (Table 5). Undoubtedly, a magnetic structure preference should be addressed with a more detailed total energy analysis (*allowing for relaxing of atom positions and lattice parameters*), which is however a difficult task for the CeFeSi-type structure (*four adjustable parameters*). Nevertheless, comparing only the $n(E_F)$ values calculated in the three magnetic structure types (Table 5), one can verify that the lowest $n(E_F)$ values are computed for the experimentally observed Mn magnetic moment arrangement (*except for BaMnGe*).

The density of states at the Fermi level almost vanishes for AFII-SrMnGe (Table 5), which predicts electron transport properties close to the metal-semiconductor limit. The dispersion curves $E(\mathbf{k})$ (Fig. 7) show an energy gap at E_F along many directions in the Brillouin zone. The main contributions to the finite $n(E_F)$ come from the valence and conduction band overlap near the centre of the Brillouin zone and also along the $\Gamma - Z$ direction.

It seems interesting to remind that electronic structure calculations have already suggested similar electron transport behaviour in the ThCr$_2$Si$_2$-type BaMn$_2$Ge$_2$ compound [29]. In order to verify these theoretical predictions, electrical resistivity measurements are in progress.

Inspecting site-decomposed and l-decomposed contributions to the total DOS (Fig. 6), one observes that the Mn d-states are strongly polarised in all cases. The calculated value of the Mn magnetic moment varies from 2.81 μ_B (MgMnGe) to 3.40 μ_B (BaMnGe). It can be also noticed that AF coupling in the (001) Mn plane substantially increases Mn magnetic moment with respect to the F arrangement (Table 5) and this increase of μ_{Mn} is accompanied by lowering of density of states in the vicinity of E_F (see, Fig. 5 and Fig. 6).

According to Fig. 1 and Fig. 4 the AFI and AFII Mn magnetic arrangements yield zero molecular fields at R and X sites. Indeed, no polarization is observed on the R and X site-projected DOS from our calculations.

Keeping in mind some limitations of the $muffin-$ tin potential in description of electronic structure and magnetism of the pseudo-layered RMnX compounds, the

agreement between theoretical and experimental values is satisfying (Table 4). Noteworthy, the KKR value obtained for MgMnGe agrees with the easy-axis model of Dascouliscou et al. ($\mu_{Mn} = 2.9(2)\mu_B$ [8]), whereas for CaMnGe the theoretical value is close to the experimental one obtained for the easy plane arrangement [4] (Table 4).

4.1.2 La$_{1-x}$Y$_x$MnSi and 'puzzling' YMnSi

In order to better understand the magnetic properties of YMnSi, KKR-CPA calculations were performed in the ferromagnetic La$_{0.2}$Y$_{0.8}$MnSi compound [7]. The computed Mn magnetic moment (2.01 μ_B) is in good agreement with the low temperature neutron diffraction study (2.1(2) μ_B). Due to their ferromagnetic environment, the Y/La and Si atoms also exhibit weak DOS polarization and experience non-zero molecular field (μ_Y = -0.06 μ_B and μ_{Si} = -0.08 μ_B).

Inspecting KKR-CPA DOS in Fig. 8 one observes E_F on the verge of the large DOS peak for the spin-down electrons, whereas in the minimum for the spin-up DOS. Hence, if the Y concentration tends to $x = 1$ in La$_{1-x}$Y$_x$MnSi, a slight decrease of spin-polarization of the Mn d-states can be expected due to the unit cell contraction. Consequently, the Fermi level would fall into a large spin-down DOS, substantially increasing the total energy. Such an electronic structure behaviour seems to be responsible for the F-AF transition occurring between $x = 0.8$ and $x = 1.0$ in the La$_{1-x}$Y$_x$MnSi solid solution [7] and detected in YMnSi [3].

Since the low temperature magnetic structure of the YMnSi compound is unknown, the KKR calculations were carried out considering three kinds of magnetic orderings: F, AFI and a hypothetical AFIII (e.g. Mn (001) ferromagnetic planes antiferromagnetically coupled).

Using the $n(E_F)$ value as criterion for stability, the AFIII magnetic ordering seems to be more favourable for YMnSi that the Mn (001) antiferromagnetic planes characterizing the other RMnX compounds (Table 5).

In Fig. 9 we observe that the manganese d-states show significant spin-polarization, yielding a magnetic moment of 1.99 μ_B, 2.29 μ_B and 1.85 μ_B in F, AFI and AFIII states, respectively. So, accounting only for the Mn-Mn distance (Table 3 and Table 5), the Mn magnetic moment value in the YMnSi compound is much smaller (even in AFI state) that those calculated for the other RMnX compounds. Thus, as discussed later, the Mn-Si distance (2.54 Å) probably controls the Mn magnetic moment magnitude in this compound.

4.2 Mn magnetic moment variation in RMnX

The evolution of μ_{Mn} versus the in-plane interatomic Mn-Mn distance (d_{Mn-Mn}) is plotted in Fig. 10. It is clearly seen that the calculated moment increases with d$_{Mn-Mn}$, in fair accordance with the experimental data. This evolution can be related to the increase of the density of states at the Fermi level and to the reduction of the Mn 3d bandwidth when d$_{Mn-Mn}$ increases [23,24]. Except for YMnSi, the correlation between μ_{Mn} and d_{Mn-Mn} is really good (Fig. 10). The Mn magnetic moment computed in the AFI

magnetic structure of YMnSi slightly better fits the values obtained for RMnX, when plotting μ_{Mn} versus d_{Mn-X} (Fig. 11).

In order to estimate the influence of the Mn-X interatomic distance on the Mn magnetic moment amplitude in the RMnX compounds, the KKR calculations were performed modifying the z_X parameter in MgMnGe (both in F and AFI state) and YMnSi (F). Such modeling does not affect the Mn-Mn distance, which only depends on lattice constant a. The obtained evolution of μ_{Mn} versus d_{Mn-X} is plotted in Fig. 12. We immediately note that μ_{Mn} strongly varies with d_{Mn-X}, from 1.5 μ_B ($d_{Mn-Si} = 2.41$ Å) to about 2.5 μ_B ($d_{Mn-Si} = 2.7$ Å) in YMnSi and from 2.5 μ_B ($d_{Mn-Ge} = 2.48$ Å) to about 3 μ_B ($d_{Mn-Ge} = 2.65$ Å) in MnMgGe.

These results apparently suggest that manganese-metalloid distances should have an essential effect on the magnetic properties of RMnX. However, the interplay with the Mn-Mn distance, seen in Fig. 10, should be also underlined.

Moreover, it is important to mention that integrating the spin-polarised d-Mn DOS in the RMnX compounds give similar number of electrons occupying d orbitals (about 5.6 electrons per Mn), whatever the nature of R, the Mn-Mn and Mn-X interatomic distances and the magnetic structure type. Let us recall that previous experimental works suggested that the Mn magnetic moment variation within the RMnX family of compounds is rather related to subsequent filling of the Mn 3d band (mostly due to the X-Mn charge transfer) when d_{Mn-X} decreases. In view of KKR results the μ_{Mn} enhancement with d_{Mn-X} is due to

the variable distribution of the Mn 3d-DOS between two spin channels (Fig. 13).

The analysis of the Mn magnetic moment dependence on Mn-X interatomic distances may be decomposed by considering two intimately related effects, namely the covalent magnetism effect (introduced by Williams et al. [34,35,33] as an alternative to the Stoner model) and the modification of the intra-atomic Coulomb repulsion with the $p-d$ hybridisation.

Recently, based on electronic structure calculations, the observed variation of μ_{Fe} with the R element valence in the RFe$_6$Ge$_6$ compounds was interpreted in terms of spin-dependent covalent interactions [36].

In all investigated RMnX compounds, whatever the R element, the spin-up and spin-down Mn 3d sub-bands are not the same and the two sub-bands do not shift in rigid way when going from the non-magnetic to ferromagnetic state (as expected from the Stoner model). The spin-polarised DOS clearly exhibit a spin-dependent hybridisation of the Mn 3d states with other electronic states. As already mentioned in Sect. 4, in the case of (La-Y)MnSi, the spin-dependent Mn 3d -Y 4d hybridisation yields a negative induced magnetic moment on the Y (La) site. Moreover, the X p - Mn 3d hybridisation is also spin-dependent, and a negative value is calculated for the Si magnetic moment in the ferromagnetic La$_{0.2}$Y$_{0.8}$MnSi compound (also observed on X-site in the F spin-polarised computations carried out in the RMnX series). Such result also reflects the mostly spin-down character of the X

$3p$ - Mn $3d$ bonding states at the X-site. Both behaviours may illustrate the covalent magnetism effect [35,33].

In order to show the effect of the Si $3p$ - Mn $3d$ hybridisation on the shape of the spin-polarised Mn $3d$ DOS, and consequently on the Mn magnetic moment, we compared (Fig. 14) the non-magnetic and ferromagnetic KKR results obtained for three different Mn-Si distances in the YMnSi compound. For the sake of clarity, only the Si $3p$ and Mn $3d$ states were displayed in Fig. 14. The Mn $3d$ density of states strongly increases in the vicinity of E_F when d_{Mn-Si} increases. At the same time, the Si $3p$ - Mn $3d$ states, presumably lying in the antibonding energy range $(0.10 < E < -0.15$ Ry), shift toward E_F. The separation between bonding and antibonding states decreases, thus indicating a reduction of the $p - d$ hybridisation. In the ferromagnetic state, the spin-up and spin-down Mn $3d$ sub-bands evolve in different and complex way and one observes the displacement of their energy barycentre toward the low and high energies, respectively. Thus, the Fermi level progressively moves into the region with a low spin-down DOS, tentatively identified as the bonding-antibonding states separation due to strong overlaps between the Mn $3d$ orbitals. Consequently, some electrons are transferred between $3d$ spin-channels (from 'down' to 'up') and the Mn magnetic moment substantially increases.

A qualitative explanation of this behaviour can be also proposed using the Kanamori's arguments [37]. The increase of the Mn-X distances is responsible for the decrease in the strength of the $p - d$ hybridisation, which results in the increase of the amplitude of wave functions on the Mn-site. Consequently, the $3d$-states on Mn become more and more localized and one can expect the increase of the repulsive intra-atomic Coulomb energy U (the parallel spin arrangement should be favoured to decrease the electrostatic interactions). In order to compensate the increase of U, there is an increase in the spin-up d-states occupation, at the expense of the spin-down d-states.

5 Conclusions

The KKR electronic structure calculations shed light on the magnetic properties of the manganese sublattice in the ternary CeFeSi-type RMnX compounds.

From analysis of the spin-dependent electronic structures, we conclude that the magnetic behaviours of these compounds can be better described in terms of the covalent magnetism than with the Stoner model. The increase of the Mn magnetic moment with interatomic distances is due to a redistribution of electrons between $3d$ spin-up and spin-down subbands.

The verification of the calculated electronic structure in the entitled compounds could be done by e.g. photoemission method. Recently, the results of X-ray photoemission spectroscopy (XPS) have been interpreted by the TB LMTO method in the similar YbMn$_2$X$_2$ compounds [42]. To our knowledge such experiments have been not performed yet for RMnX compounds.

The influence of the interatomic distances, intraplanar Mn-Mn and particularly Mn-X, on the polarization of the

Mn $3d$ states (the amplitude of μ_{Mn}), well supports the experimentally observed evolution in the RMnX series.

The electronic structure calculations in $R(=$Mg-Ba$)$MnX silicides and germanides yield μ_{Mn} in rather good agreement with the experimental ones (Fig 15).

The computations have also revealed that precise crystallographic data (especially atomic coordinates controlling d_{Mn-X} distances) are of primary importance to allow for phenomenological predictions of magnetic behaviours in these compounds from simple steric criteria.

Comparing DOS computed in the F, AFI and AFII states, we have found that the lowest value of $n(E_F)$ corresponds to experimentally observed magnetic orderings (i.e. AF (001) Mn planes) in most RMnX compounds. Using the same $n(E_F)$ criterion, in YMnSi (high pressure compound), the KKR calculations favour the occurrence of ferromagnetic (001) Mn planes (antiferromagnetically coupled along the c-axis), as suggested in previous experimental works on La$_{1-x}$Y$_x$MnSi solid solution. The KKR-CPA calculations of the ferromagnetic La$_{0.2}$Y$_{0.8}$MnSi compound resulted in a Mn magnetic moment value in very good agreement with the experimental data.

In another way, unlike the strong magnetic properties of the RMnX compounds, the ground state of YFeSi was determined to be non-magnetic, which is in excellent agreement with the Mössbauer data.

Finally, it would be highly desirable to perform electronic structure calculations [38,39] for RMnX compounds containing $4f$ element due to a wide variety of their magnetic behaviours [40,41].

Table 1. Crystallographic parameters of the CeFeSi-type structure (space group P4/nmm, $a \approx 4$ Å, $c \approx 7$Å)

Atom	Position	Point symmetry	x	y	z
Ce	2(c)	$4mm$	$\frac{1}{4}$	$\frac{1}{4}$	≈ 0.66
Fe	2(a)	$42m$	$\frac{3}{4}$	$\frac{1}{4}$	0
Si	2(c)	$4mm$	$\frac{1}{4}$	$\frac{1}{4}$	≈ 0.18

Table 2. Lattice parameters (in Å) and atomic positions of the CeFeSi-type RMnX compounds. Mn-Mn interatomic distance ($d_{Mn-Mn} = \sqrt{2}a$) is given in Å.

Compound	a (Å)	c (Å)	z_R	z_X	d_{Mn-Mn}	Ref.
MgMnGe	3.949	6.535	0.655	0.252	2.79	[5]
CaMnGe	4.227	7.201	0.661	0.220	2.99	[4,8,16]
SrMnGe	4.381	7.482	0.667	0.206	3.10	[8,9,16]
BaMnGe	4.507	7.893	0.668	0.190	3.19	[8,9,16]
CaMnSi	4.172	7.121	0.669	0.213	2.95	[4]
YMnSi*	3.970	7.150	0.67	0.22	2.81	[3]

* extrapolated atomic coordinates

Acknowledgments

References

1. Szytuła A, Leciejewicz L, in: Gschneider K A and Eyring L (Eds.), *Handbook on the Physics and Chemistry of Rare Earth*, vol. **12**, Elsevier, Amsterdam, 1989, p.133.

2. Szytuła A, in: K.H.J. Buschow (Ed), *Handbook of Magnetic Materials*, vol. **6**, Elsevier, Amsterdam, 1991, p. 85.

3. Kido H, T. Hoshikawa, M. Shimida, M. Koizumi, Phys. Stat. Sol. (a) **88**, (1985) K39.

Table 3. KKR d-DOS at the Fermi level for T-site (in states/Ry) and Stoner products $In(E_F)$ for RMnX. The corresponding interatomic distances, $d_{T-X} = \sqrt{2}a$ and $d_{T-X} = \sqrt{\frac{a^2}{4} + z_X^2 c^2}$, are given in Å.

Compound	d_{T-T}	d_{T-X}	$n_d(E_F)$	$In(E_F)$
MgMnGe	2.79	2.57	43.5	1.39
CaMnSi	2.95	2.58	58.6	1.81
CaMnGe	2.99	2.64	64.2	1.96
SrMnGe	3.10	2.67	72.8	2.26
BaMnGe	3.19	2.71	78.2	2.40
YCrSi*	2.76	2.55	21.5	0.72
YMnSi**	2.81	2.54	43.6	1.45
YFeSi**	2.75	2.32	19.6	0.68

* hypothetical structure

** extrapolated atomic coordinates

Table 4. Experimental and calculated Mn magnetic moments (in μ_B) for antiferromagnetic RMnX compounds.

Compound	μ_{exp}	μ_{cal}	Ref.
MgMnGe	2.9(2) *)	2.81	[8]
	3.3(1) **)		[5]
CaMnGe	3.34(3) tilted	3.15	[4]
	3.8(2) *)		[8]
SrMnGe	3.29(6) **)	3.31	[8]
BaMnGe	3.70(6) **)	3.40	[8]
CaMnSi	2.84(8) *)	3.02	[8]
	3.27(4) *)		[5]

* parallel c-axis

** perpendicular c-axis

Table 5. KKR results, Mn magnetic moment μ_{Mn} (in μ_B) and DOS at E_F $n(E_F)$ (in states/Ry/f.u.) in the RMnX compounds in ferromagnetic (F) and antiferromagnetic (AFI, AFII) states. The values in bold correspond to the results obtained accounting for experimentally observed magnetic structure.

Compound	μ_{Mn}			$n(E_F)$		
	F	AFI	AFII	F	AFI	AFII
MgMnGe	2.19	**2.81**	2.69	70.5	**63.4**	70.5
CaMnGe	2.50	**3.15**	3.15	129.6	**21.7**	24.7
SrMnGe	3.09	3.33	**3.31**	105.8	104.1	**0.1**
BaMnGe	3.22	3.43	**3.40**	115.9	3.5	**15.3**
CaMnSi	2.06	**3.02**	2.59	109.7	**33.1**	105.6
YMnSi	1.99	2.29	1.85 *	91.9	81.2	66.1

* AFIII ordering

4. Welter R, Venturini G, Ressouche E, Malaman B, Solid State Comm. **97(6)**, (1996) 503.

5. Welter R, Malaman B, Venturini G, Solid State Comm. **108** (12), (1998) 933.

6. Welter R, Ijjaali I, Venturini G, Malaman B, J. Alloys Comp. **265**, (1998) 196.

7. Ijjaali I, Welter R, Venturini G, Malaman B, Ressouche E, J. Alloys Comp. **270**, (1998) 63.

8. Dascoulidou A, Müller P, W. Bronger W, Z. Anorg. Allg. Chem. **624**, (1998) 124.

9. Welter R, Venturini G, Ijjaali I, Malaman B, J. Magn. Magn. Mater. **205**, (1999) 221.

10. Klosek V, Vernière A, Ouladdiaf B, Malaman B, J. Magn. Magn. Mater. **256**, (2003) 69.

11. Bansil A, Kaprzyk S, Tobola J, in: W.H. Bulter, P.H. Dederichs, A. Gonis, R.L. Weaver (Eds.), *Applications of Multi-*

ple Scattering Theory in Material Science, Vol. **252**, MRS, Pittsburgh, 1992, p. 505.

12. Bansil A, Kaprzyk S, Mijnarends P E, Tobola J, Phys. Rev. B **60**, (1999) 13396.

13. Kaprzyk S, Acta Phys. Pol. A **91**, (1997) 135.

14. von Barth U, Hedin L, J. Phys. C **5**, (1972) 1629.

15. Bodak O I, Gladyshevskii E I and Kripyakevich P I, Jour. Struct. Chem., **11** (2), (1970) 283.

16. Villars P, *Pearson's Handbook: Crystallographic Data for Intermetallic Compounds*, ASM International, 1997.

17. Kaprzyk S, Mijnarends P E, J. Phys. C **5**, (1972) 1629.

18. Kaprzyk S, Bansil A, Phys. Rev. B **42**, (1990) 7358.

19. Gelatt C D, Williams A R, Moruzzi V L, Phys. Rev. B **27**, (1983) 2005.

20. Matar, Eyert, J. Magn. Magn. Mater. **166**, (1997) 321.

21. Bisi O, Calandra C, J. Phys. C: Solid State Phys. **14**, (1981) 5479.

22. Klosek V, Ph. D. Thesis, Université H. Poincaré - Nancy I (2002).

23. Weijs P J W, Czyzyk M T, Fuggle J C, Speier W, Sarma D D, Büschow K H J, Z. Phys. B - Condensed Matter **78**, (1990) 423.

24. Johansson B, Brooks M S S, in: K.A. Gschneider, L. Eyring, G.H. Lander, G.R. Choppin (Eds.), *Handbook on the Physics and Chemistry of Rare Earths*, vol. **17**, North Holland, Amsterdam, 1993, p. 149.

25. Kulatov E, Veselago V and Vinokurova L, Acta Phys. Pol. A **77**, (1990) 709.

26. Welter R, Ph. D. Thesis, Université H. Poincaré - Nancy I (1994).

27. Ishida S, Asano S, Ishida J, J. Phys. Soc. Japan., **55**, (1986) 936.

28. Ijjaali I, Venturini G, Malaman B, J. Alloys Comp. **279**, (1998) 102.

29. Tobola J, Malaman B, Venturini G, Acta Phys. Pol. A **97** (5), (2000) 761.

30. Janak J F, Phys. Rev. B **16**, (1977) 255.

31. Brooks M S S, Eriksson O, Johansson B, J. Phys. : Condens. Matter **1**, (1989) 5861.

32. Brooks M S S, Nordström L, Johansson B, J. Phys. : Condens. Matter **3**, (1991) 2357.

33. Kübler J and Eyert V, in Cahn R W, Haasen P and Kramer E J (Eds.), *Materials Science and Technology: A Comprehensive Treatment*, vol. **3A**, VCH, Weinheim, 1992, p. 1.

34. Williams A R, Zeller R, Moruzzi V L, Gelatt Jr. C D, Kübler J, J. Appl. Phys. **52**, (1981) 2067.

35. Williams A R, Moruzzi V L, Gelatt Jr. C D, Kübler J, Schwarz K, J. Appl. Phys. **53**, (1982) 2019.

36. Mazet T, Tobola J, Malaman B, Eur. Phys. J. B **34**, (2003) 131.

37. Kanamori J, Prog. Theor. Phys. Suppl. No **101** (1), (1990).

38. Brooks M S S, Physica B **130**, (1985) 6.

39. Eriksson O, Brooks M S S, Johansson B, Phys. Rev. B **41**, (1990) 7311.

40. Welter R, Venturini G, Malaman B, J. Alloys Compd. **206**, (1994) 55.

41. Welter R, Venturini G, Ressouche E, Malaman B, J. Alloys Compd. **228**, (1995) 59.

42. Szytula A, Jezierski A, Penc B, Hofmann M, Campbell S J, J. Alloys Compd. **363**, (2004) 46.

Fig. 1. Tridimensional views of the CeFeSi-type and ThCr$_2$Si$_2$-type structures

Fig. 2. KKR non-spin-polarised DOS for the RMnX compounds. The upper panel is total DOS. The s, p and d contributions are plotted by dotted, solid thick and solid thin lines, respectively.

Fig. 3. KKR non-polarised total and T-site DOS for YTSi (T= Cr, Mn, Fe).

Fig. 4. Tridimensional views of the magnetic structures of the CeFeSi-type RMnX silicides and germanides.

Fig. 5. KKR spin-polarised DOS for the ferromagnetic RMnX compounds.

Fig. 6. KKR spin-polarised DOS for the antiferromagnetic RMnX compounds.

Fig. 7. The electronic dispersion curves E($\mathbf{k}$) in the SrMnGe antiferromagnet. For a sake of clarity only bands in the vicinity of the Fermi level were plotted.

Fig. 8. KKR-CPA spin-polarised DOS for La$_{0.2}$Y$_{0.8}$MnSi. Mn-DOS is plotted by dotted line.

Fig. 9. KKR spin-polarised DOS for YMnSi in F, AFI and AFIII states. Mn-DOS is plotted by a thick line.

Fig. 10. The calculated Mn magnetic moment versus the Mn-Mn distance in RMnX. A line is added as a guide to the eye.

Fig. 11. The calculated Mn magnetic moment versus the Mn-X distance in RMnX. A line is added as a guide to the eye.

Fig. 12. Modeling of the Mn magnetic moment variations with the Mn-X distance in YMnSi (in F state) and MgMnGe (in AFI state). Only z_X was modified in the KKR simulations.

Fig. 13. Number of electrons filling spin-up and spin-down Mn d-DOS versus the Mn-Mn distances in the RMnX compounds. Lines are added as a guide to the eye.

Fig. 14. KKR non-spin-polarised (left panel) and spin-polarised (right panel) DOS in the CeFeSi-type YMnSi simulated at three different Mn-Si interatomic distances (d_{Mn-Si}, given in Å). For a sake of clarity only Mn d-states (thin line) and Si p-states (thick line) are plotted.

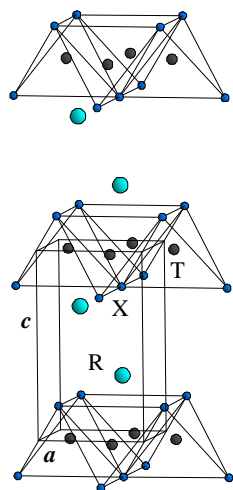**Fig. 15.** Comparison of experimental (with error bars) and theoretical values of the Mn magnetic moment in RMnX compounds (see text).
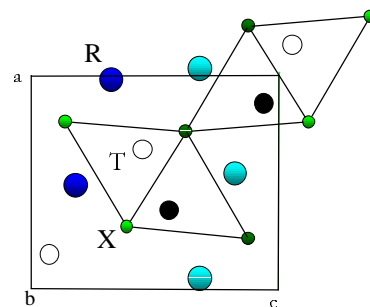
CeFeSi

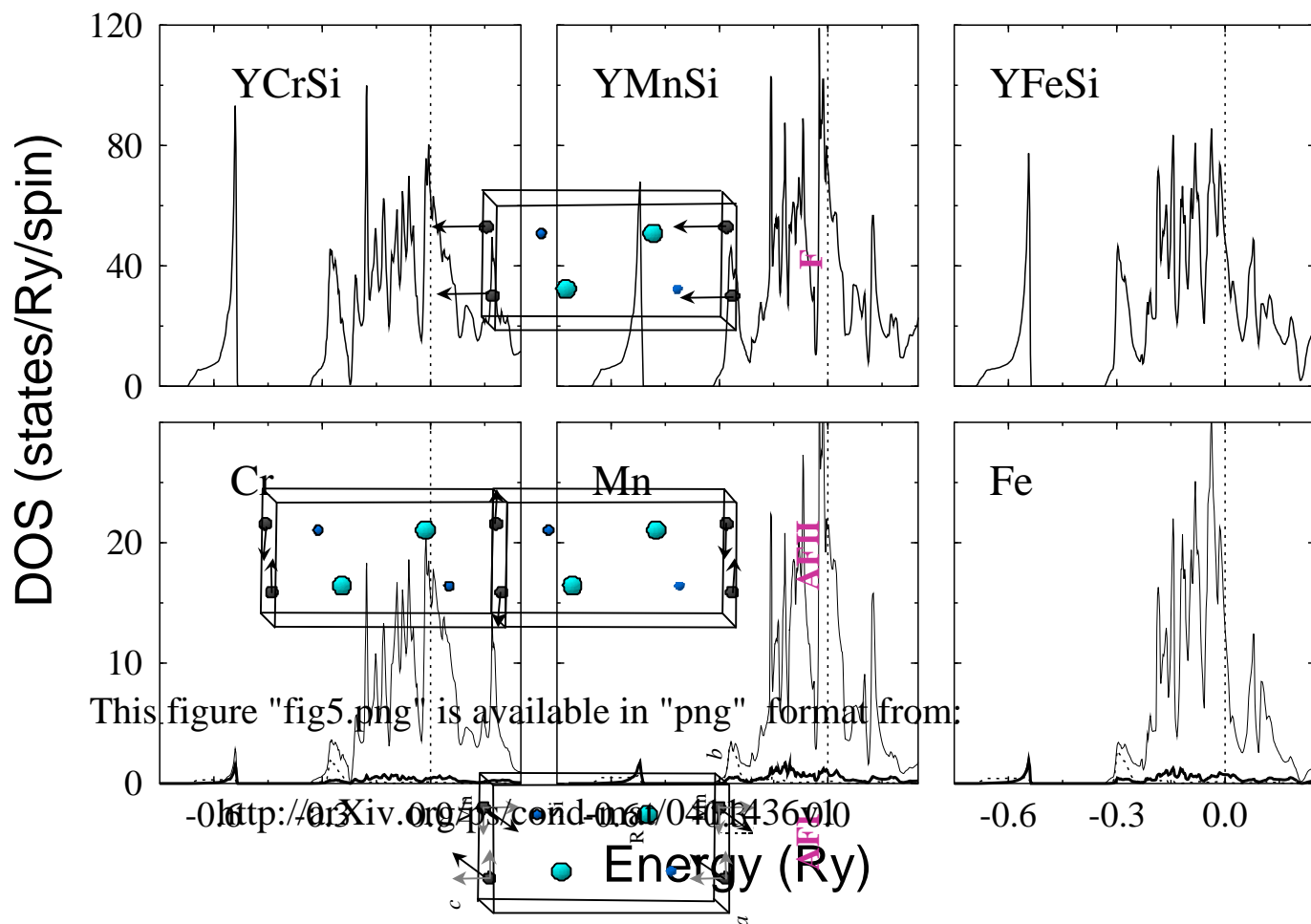ThCr$_2$Si$_2$

TiNiSi
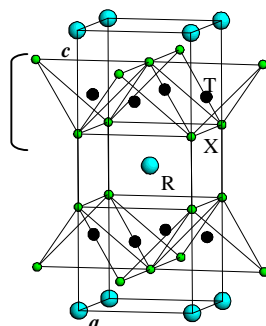
'W' block

'BaAl$_4$' block

This figure "fig6.png" is available in "png" format from:

http://arXiv.org/ps/cond-mat/0411436v1

This figure "fig7.png" is available in "png" format from:

http://arXiv.org/ps/cond-mat/0411436v1

DOS (states/Ry/spin)

Intergrated *d*-DOSonMn

μ_{Mn} (μ_B)

3.5
4.0
'up'
BaMnGe
SrMnGe
CaMnGe
CaMnSi
SrMnGe
('up + down')/2
BaMnGe
3.5
3.0
MgMnGe
CaMnSi
CaMnGe
2.5
2.0
$d_{Mn-Si} = 2.35$
20
MgMnGe
YMnSi
'down'
YMnSi

$d_{Mn-Si} = 2.35$

Mn magnetic moment

4.5

4.0

$d_{Mn-Si} = 2.51$

30

20

La $_{0.5}$ Y MnSi (Å)

3.5

d_{Mn-Mn} (Å)

2.7 2.8 2.9 3.0 3.1 3.2

2.4 2.5 2.6 2.7 2.8

$d_{Mn-Si} = 2.51$

d_{Mn} (Å)

MgMnGe (AF)

3.0

2.8

2.5

2.4

2.0

$d_{Mn-Si} = 2.65$

$d_{Mn-Si} = 2.65$

expt. (1)
expt. (2)
present KKR

-0.6   0.0   Energy (Ry)

MgMnGe
CaMnSi
CaMnGe
SrMnGe
YMnSi (F)
BaMnGe
YMnSi

2.6

1.6

2.0

Mn magnetic moment

DOS (states/Ry)

30

F
AFI
AFIII

60
30
2.4   2.5   2.6   2.7

0
d_{Mn-X}

30
60

DOS (states/Ry)

60
90

-0.6   -0.4   -0.2   0.0   0.2
-0.6   -0.4   -0.2   0.0   0.2
-0.6   -0.4   -0.2   0.0   0.2

Energy (Ry)
Energy (Ry)